

Pose estimation and mapping based on IMU and LiDAR

Janis Kaltenthaler Helge A. Lauterbach Dorit Borrmann
Andreas Nüchter (andreas.nuechter@uni-wuerzburg.de)

*Informatics VII: Robotics and Telematics,
Julius-Maximilian-University Würzburg, Am Hubland, D-97074
Würzburg, Germany*

Abstract: In the field of autonomous motion and mapping, estimating the position and orientation of a moving body is of high significance. This includes in particular the latest information about acceleration, speed, traveled distance and orientation. A wide range of different technologies exists that can be applied for this purpose. In case the state determination requires the use of inertial sensors only, it is well known that these types of sensors tend to drift with time. This leads to increasing errors in the calculated trajectory, which is unacceptable if precise position information is required such as for mapping. In this paper we present a method which significantly enhances the position estimation of inertial sensors by using a 2D *light detection and ranging* (LiDAR) sensor.

Keywords: Integration of Sensors, Sensor Fusion and Sensor Systems, Trajectory Tracking, Localization and SLAM, Parameter Estimation, Identification and Optimization, Navigation Systems, Remote sensor data acquisition

1. INTRODUCTION

A variety of different sensors and measurement methods exist to acquire motion data, such as acceleration, velocity, position and orientation data. Every technique involves certain inaccuracies and situations where they fail. A *global navigation satellite systems* (GNSS) receiver is only working precisely in the presence of sufficient radio reception thus neither underground nor inside buildings. Odometry is only suitable for a wheeled system on a smooth surface. Laser scanning localization methods require a known environment or at least enough features in their surroundings.

In situations where an absolute localization is not required and a relative localization towards a predefined position is sufficient, *inertial measurement units* (IMUs) are suitable. Possible use cases include bridging weak GNSS signals, tracking relative positions underground or any other situation where conventional techniques are failing. An IMU combines various inertial sensors for acceleration, angular rate and magnetism along three orthogonal axes. The benefit of measuring motion data through accelerometers is the constant availability of the measured values, i.e. accelerating forces initiated by motion. Due to this fact acceleration is measurable everywhere and there is no difference between over- and underground or in- and outside of buildings. Integrating the measured linear acceleration after compensating gravitational forces results in velocity respectively relative position.

However, minimal errors in the acceleration measurement result in large deviations in the calculated relative position due to double integration. In this paper we present a method which significantly reduces the drift of low-cost IMUs using a low-cost LiDAR. At this point, imagine

a UAV that has to navigate or map inside a building. GNSS will have no reception and cameras will only work in suitable lighting conditions and with sufficient features. LiDAR, in combination with an IMU, which is usually installed anyway, can significantly improve the position estimation by IMUs. In addition, LiDAR provides the necessary technology to simultaneously generate a 3D map of the environment. The following demonstrates how to accomplish such a task even with inexpensive technology.

First, we introduce an effective calibration method for IMUs. After that, we present a complementary filter, which enables a reliable determination of the orientation using the IMUs even during dynamic motion. Then we apply our method for improving the position estimation of an IMU using a LiDAR. Finally, we evaluate the designed methods by generating 3D point clouds using the computed trajectories and comparing them to data acquired with a terrestrial LiDAR.

2. RELATED WORK

Various publications deal with fusion of data acquired by an IMU and another type of sensor or data to obtain more precise pose information. The research by Hellmers et al. (2016) describes the fusion of position data obtained from an IMU and an ultra wide band (UWB) system to allow the localization of a mobile platform inside buildings. For fusion they use a modified version of the extended Kalman filter (EKF), the so-called iterated Kalman filter (IKF). In Wendel (2011) the author describes in detail the fusion of measurement data obtained by IMU and GNSS. He explicitly discusses the use of an EKF and a sigma point Kalman filter to obtain a precise position estimation. Emter and Petereit (2019) present an approach

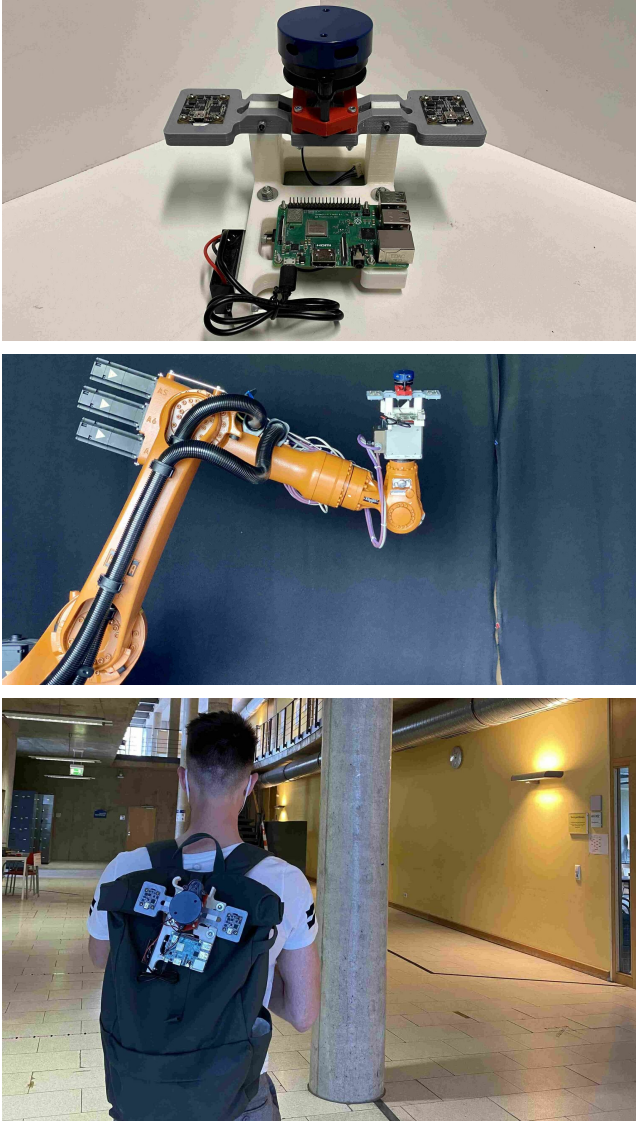


Fig. 1. Measurement setup in form of a 6-axis jointed-arm robot manufactured by KUKA and classification KR16. The IMUs and the LiDAR are mounted on a 3D printed mount (top) and this mount is attached to the wrist of the robot (middle), respectively to a backpack (bottom).

to join multiple absolute and relative pose estimates from various sensors using an EKF. They implement a stochastic cloning to overcome the violation of the independence assumption when using multiple relative measurements and demonstrate their approach on data from IMU, GNSS, wheel odometry and scan matching using 3D LiDAR measurements. While fusion of multiple sensor data is shown to improve the localization capabilities, this paper presents a method that produces reliable position estimates even when odometry and GNSS are not available. In other publications the fusion of IMU internal measurements, i. e. acceleration and angular velocity, in order to get the attitude of the device is discussed. A description and a review of fusing these data using the complementary Kalman, Mahony or Madgwick filters is available online ¹. The orientation filter developed by Madgwick (2010) uses

accelerometer-, gyroscope- and magnetism-measurements, obtained with a single IMU, to estimate attitude information. Madgwick’s filter uses, among other information, the direction of Earth’s gravitational acceleration to determine the orientation of the IMU. An external acceleration, triggered by e.g a movement, distorts the direction of the gravitational acceleration vector, which leads to incorrect orientation estimations. In our case, the orientation estimation must be as accurate as possible for all types of movements. Therefore, we gratefully use the complementary filter developed by Valenti et al. (2015), which overcomes this limitation (cf. section 5). For calibrating our IMUs, we thankfully use a method envolved by Tedaldi et al. (2014) (cf. section 4).

Only a few publications deal with trajectory tracking by using a single IMU or fusion of multiple IMU data. Wongwirat and Chaiyarat (2010) determine the position of a robot during a movement using an IMU with moderate success. Especially because they do not verify if gravity is compensated correctly during “no motion” periods, the results for speed and distance are distorted. In our work we investigate the problem that gravity causes. McCall (2019) describes the fusion of data obtained from 6 IMUs to track the position of a moving vehicle. He shows that the fusion increases the accuracy of acceleration measurements.

3. MEASUREMENT SETUP

For experiments within this work we use two low-cost IMUs manufactured by *Phidgets*. Their type definition is stated as PhidgetSpatial Precision 3/3/3 High Resolution ². In addition, we use a low-cost X2 LiDAR manufactured by *YDLIDAR* ³. This sensor has a range of 12m and records data in a field of view of 360 degrees. To record and process the data we use a framework called *Robot Operating System* (ROS) ⁴, that provides drivers for the sensors. An industrial robot from *KUKA* is used to hold the devices with different orientations and to perform exact movements on them. Using a 3D printed mount, the sensors are attached to its wrist as shown in Fig. 1. Note that we only use the data from one IMU, the other one is mounted only for backup reasons. One IMU provides us with linear acceleration measurements in form of:

$${}^{S_a} \hat{\mathbf{a}} = [a_x \ a_y \ a_z]^T \quad (1)$$

and angular velocity measurements in form of:

$${}^{S_\omega} \hat{\boldsymbol{\omega}} = [\omega_x \ \omega_y \ \omega_z]^T. \quad (2)$$

The LiDAR provides us with j distance measurements per revolution in form of:

$${}^S \mathbf{r} = [r_1 \ r_2 \ \dots \ r_j]^T. \quad (3)$$

The superscript S_a denotes the accelerometer frame, S_ω the gyroscope frame and S the body frame. For simplicity, we assume that the coordinate system of the LiDAR already coincides with the body frame S . This assumption does not introduce a large error due to the fact that the 2D scan plane of the LiDAR is aligned parallel to the XY -plane of the IMUs. In the following sections, the individual components of our method, shown in Fig. 2, are explained.

² <https://www.phidgets.com/?catid=10&pcid=8&prodid=1158>

³ <https://www.ydlidar.com/products/view/6.html>

⁴ <https://www.ros.org>

¹ <http://www.olliv.eu/2013/imu-data-fusing/>

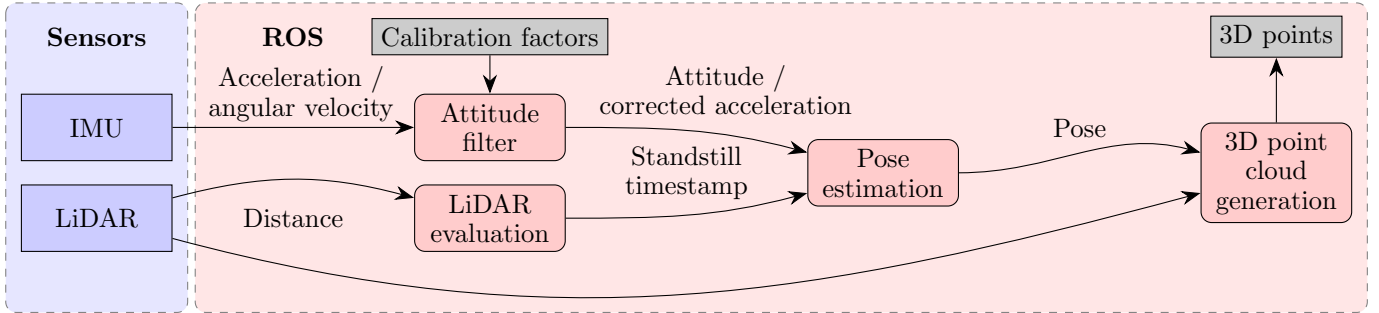


Fig. 2. Diagram showing the operation of our system.

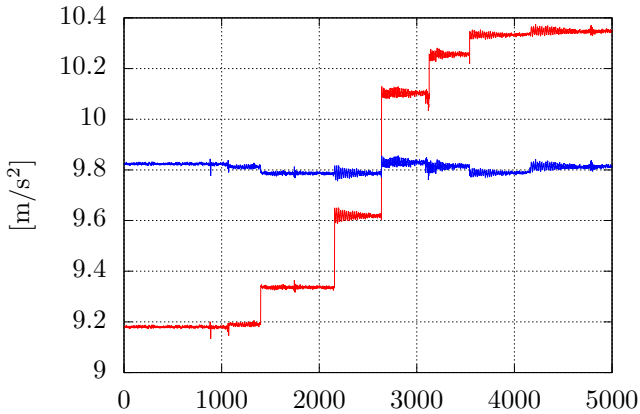


Fig. 3. The x -axis shows the number of measurements. The y -axis shows the gravitation in $\frac{m}{s^2}$. Shown are the measured gravitations at different orientations before (red line) and after (blue line) calibration. For the sake of clarity, the acceleration data during the change of orientation was removed.

4. IMU CALIBRATION

To estimate the position as accurately as possible using the IMU data, the IMUs must be calibrated in advance. It is well known that sensors of this construction type suffer from various sources of error. The following deterministic errors are treated with the corresponding scaling and rotation matrices:

- In the ideal case, the three sensor axes of the accelerometer, respectively the gyroscope, will each form an orthogonal coordinate system and coincides with the body frame S . Due to assembly inaccuracies, both the accelerometer frame and the gyroscope frame form two distinct (i.e., misaligned), non-orthogonal, frames S_a and S_ω . In addition, the sensor coordinate systems of the accelerometer and the gyroscope differ from the body frame S . T defines the orthogonalization of the individual sensor axes to an orthogonal frame, as well as the rotation of the two frames to the body frame, whereby the latter only applies to the gyroscope, since the orthogonalized accelerometer frame defines the body frame S in our case.
- The scaling factors for converting the digital measured value of the sensors into the physical value acceleration, respectively angular velocity, are different

for different instances of the same sensors. K scales the individual sensor axes.

- Both the accelerometers and the gyroscopes are affected by biases. The bias vector is defined by b .

To minimize these errors, we use the approach developed by Tedaldi et al. (2014) and refer to their detailed mathematical description. In the following, we fundamentally discuss the procedure.

The corrected measurements are obtained with the following functions:

$${}^S \mathbf{a} = T_a K_a ({}^{S_a} \hat{\mathbf{a}} + \mathbf{b}_a) \quad (4)$$

$${}^S \boldsymbol{\omega} = T_\omega K_\omega ({}^{S_\omega} \hat{\boldsymbol{\omega}} + \mathbf{b}_\omega). \quad (5)$$

To determine the calibration factors, cost functions are introduced, which are minimized using the Levenberg-Marquardt algorithm. A minimum of nine measurements with different orientations are required for a unique solution. There were about 30 in our case. The robot shown in Fig. 1 was used for precise alignment of the sensors. In addition, efforts were made to ensure that the recorded measurements were equally distributed over all possible orientations. The results of the calibration are shown exemplarily in Fig. 3. Gravity was measured at different orientations. The red line shows the results before calibration and the blue line after calibration. The positive effect of the calibration on the measurement data acquisition is obvious as it leads to gravity remaining almost constant. In the uncalibrated case, the following gravity was measured, stated with mean value and associated standard deviation:

$$|{}^S \hat{\mathbf{a}}| = (9.846 \pm 0.5088) \frac{m}{s^2}, \quad (6)$$

after calibration:

$$|{}^S \mathbf{a}| = (9.808 \pm 0.01677) \frac{m}{s^2}. \quad (7)$$

The calibration, corrects the measured acceleration values very close to the actual gravity of $g = 9.807 \frac{m}{s^2}$. Additionally the measurement error in this example decreased by a factor of ≈ 30 .

5. COMPLEMENTARY FILTER FOR ORIENTATION DETERMINATION

Later, we use the acceleration measurements to calculate the velocity and traveled distance of the IMU in its sensor frame. To do this, it is necessary to eliminate the effects of Earth's gravity from the data to obtain the relative acceleration acting on the sensor. This requires knowing the exact orientation of the sensor with respect to the gravity

vector, even during periods of strong acceleration. We use the filter of Valenti et al. (2015) for determining the orientation, since it provides reliable results even during highly dynamic motion. The following deals with the basic functionality of the filter. Consecutively, the filter calculates for each time step two orientation quaternions, representing the relative rotation between the global (Earth) coordinate system and the body frame S , first, from the direction of the measured acceleration vector directly and second, by integrating the angular velocities over time together with an initial orientation. Subsequently, the quaternion calculated using the gyroscope data is corrected with the quaternion of the acceleration data, depending on the acceleration applied. Accordingly, during periods of high dynamics, the values of the gyroscope are trusted more, and in the static case, the values of the accelerometer. The resulting orientation quaternion is referred to as ${}^G_S\mathbf{q}$ and defines the rotation from the body frame S to the global coordinate system G . Interested readers are referred to the work of Valenti et al. (2015) for a detailed description of the algorithm.

6. USING A LIDAR TO REDUCE THE IMU DRIFT

The main objective of this work is to reduce the drift of IMUs with the help of data acquired by a LiDAR. This section presents the logic we developed for reliably detecting standstill phases based on the LiDAR data and demonstrates how this improves IMU position estimation.

6.1 Evaluation of LiDAR data

The LiDAR provides us with j distance measurements ${}^S\mathbf{r}$ per revolution, hence $\dim({}^S\mathbf{r}) = j$. For each time step t , the changes in the j distances compared to the previous step $t - 1$ are evaluated and accumulated to the last i values:

$$\mathbf{r}_{\Sigma,t} = \sum_{k=t-i}^t {}^S\mathbf{r}_{k-1} - {}^S\mathbf{r}_k. \quad (8)$$

The last i vectors \mathbf{r}_{Σ} are stored. Following each time t , it is then determined how many components of the last i vectors \mathbf{r}_{Σ} were within a margin ε . In our case we set $\varepsilon = 0.1$. Thus, we count the number of distances, which have not changed or barely changed in the last i measurements of the LiDAR. Let this quantity be j_{ε} .

It can occur that all i last distance measurements of an index j were faulty, hence $r_{\Sigma,t,j} = 0$. A faulty measurement occurs when the LiDAR receives no return signal and thus determines no distance value. These measurements are not being counted in j_{ε} . Let j_{faulty} be the number of unevaluable measurements. As a result, we calculate now a factor m that allows us to determine the type of movement:

$$m = \frac{j_{\varepsilon}}{j - j_{\text{faulty}}}. \quad (9)$$

It now holds for $m \approx 1$ with a high degree of certainty that the LiDAR is at a standstill. Whereas for $m \approx 0$ it is assumed that the LiDAR is moving. In our case, we assume a standstill for $m > 0.8$. With this, we determine the exact time when the LiDAR is not moving, denoted as t_{stop} .

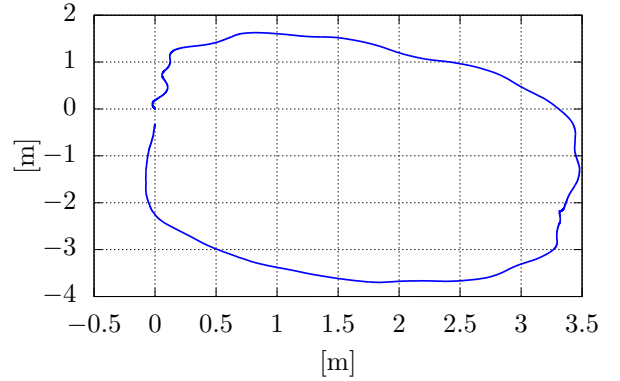


Fig. 4. The x -axis shows the translation in the x direction in m. The y -axis shows the translation in the y direction in m. In the figure, a resulting trajectory is shown using the presented method. A circular path with identical start and target position was traversed in this case. For the sake of clarity, the z coordinates are not shown.

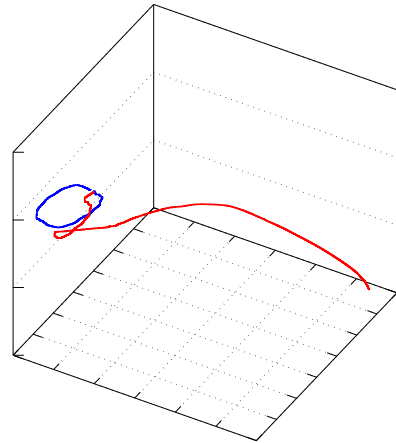


Fig. 5. The trajectory from Fig. 4 in three-dimensional space. For comparison, the resulting trajectory has also been plotted (red line), which arises if the correction by the LiDAR data is omitted. In both cases, the same calibrated measured values of the IMU were used.

6.2 Position estimation

The IMU provides us with the corrected acceleration measurement values ${}^S\mathbf{a}$ in the body frame. These values are now first rotated into the global coordinate system:

$${}^G\mathbf{a}_q = {}^G_S\mathbf{q} \otimes {}^S\mathbf{a}_q \otimes {}^G_S\mathbf{q}^*, \quad (10)$$

where ${}^G_S\mathbf{q}^*$ is the conjugate quaternion, \otimes the quaternion multiplication, and ${}^S\mathbf{a}_q$ the pure quaternion of ${}^S\mathbf{a}$. A pure quaternion, denoted with subscript q , is defined as follows:

$$\mathbf{x}_q = [0 \ \mathbf{x}]^T. \quad (11)$$

The relative acceleration of the sensor is obtained as follows:

$${}^G\mathbf{a}_{\text{rel}} = {}^G\mathbf{a} - \mathbf{g}. \quad (12)$$

Here $\mathbf{g} = [0 \ 0 \ g]^T$ represents the gravitational vector. Using ${}^G\mathbf{a}_{\text{rel}}$, the velocity and distance traveled are now calculated starting from an initial value by temporal

integration. Additionally, we introduce an uncertainty vector $\boldsymbol{\nu}$ at this point.

$${}^G\mathbf{v}_t = {}^G\mathbf{v}_{t-1} + ({}^G\mathbf{a}_{\text{rel},t} - \boldsymbol{\nu})\Delta t \quad (13)$$

$${}^G\mathbf{s}_t = {}^G\mathbf{s}_{t-1} + {}^G\mathbf{v}_t\Delta t \quad (14)$$

Here Δt denotes the time difference between the measurements at t and $t - 1$. With the help of the evaluation of the LiDAR data, we now determine $\boldsymbol{\nu}$, between two times of complete standstill. For the associated t_{stop} we assume that the LiDAR does not move anymore, consequently ${}^G\mathbf{v} \stackrel{!}{=} 0$. Therefore, we now calculate $\boldsymbol{\nu}$ as follows for the preceding motion phase:

$$\boldsymbol{\nu} = \frac{{}^G\mathbf{v}_{t_{\text{stop}}}}{\Delta tk}, \quad (15)$$

where k is the number of measured values during the motion phase and ${}^G\mathbf{v}_{t_{\text{stop}}}$ the error-prone velocity determined by the IMU at the time of standstill. This allows us to correct the measured acceleration values during the motion phase according to Eq. (13) afterwards.

6.3 3D Point Cloud generation

Using the calculated positions and orientations, the captured 2D scans are now rotated and translated to create a 3D point cloud. Here ${}^S\mathbf{p}_{t,j}$ denotes the point which is calculated from the corresponding distance measurement in the body frame. ${}^G\mathbf{p}_{t,j}$ denotes this point, which was transformed into the global coordinate system. As follows, those points being calculated:

$${}^S\mathbf{p}_{t,j} = \begin{bmatrix} r_{t,j} \sin(j\Delta\alpha) \\ r_{t,j} \cos(j\Delta\alpha) \\ 0 \end{bmatrix}, \quad (16)$$

$${}^G\mathbf{p}_{q,t,j} = {}^G\mathbf{q}_t \otimes {}^S\mathbf{p}_{q,t,j} \otimes {}^G\mathbf{q}_t^* + {}^G\mathbf{s}_{q,t}, \quad (17)$$

where the angular distance between each distance measurement, given by the LiDAR specifications, is defined as $\Delta\alpha$.

7. EXPERIMENTS

To demonstrate the potential of our algorithm, the apparatus shown in Fig. 1 (top) was loosely attached to a backpack (bottom). Using this, we walked through our institute building and recorded the raw data from LiDAR and the calibrated measurements from the IMU during this time. Due to the human walking gait the device ‘‘wobbled’’ during the data recording. Every few meters we stopped for a moment so the LiDAR could detect a standstill. The evaluation of the data was performed in post-processing.

7.1 Pose estimation

To demonstrate that our method improves the position estimation of the IMU, we walked a circular route. Care was taken to ensure that the start and end positions match. The resulting position estimates are shown in Fig. 4. As it can be seen, there is only a slight deviation of the end position from the start position.

For comparison, the same acceleration measurements were used to determine the position without the help of the LiDAR. In Fig. 5, these are plotted as a red line, showing an enormous difference to the position estimation with

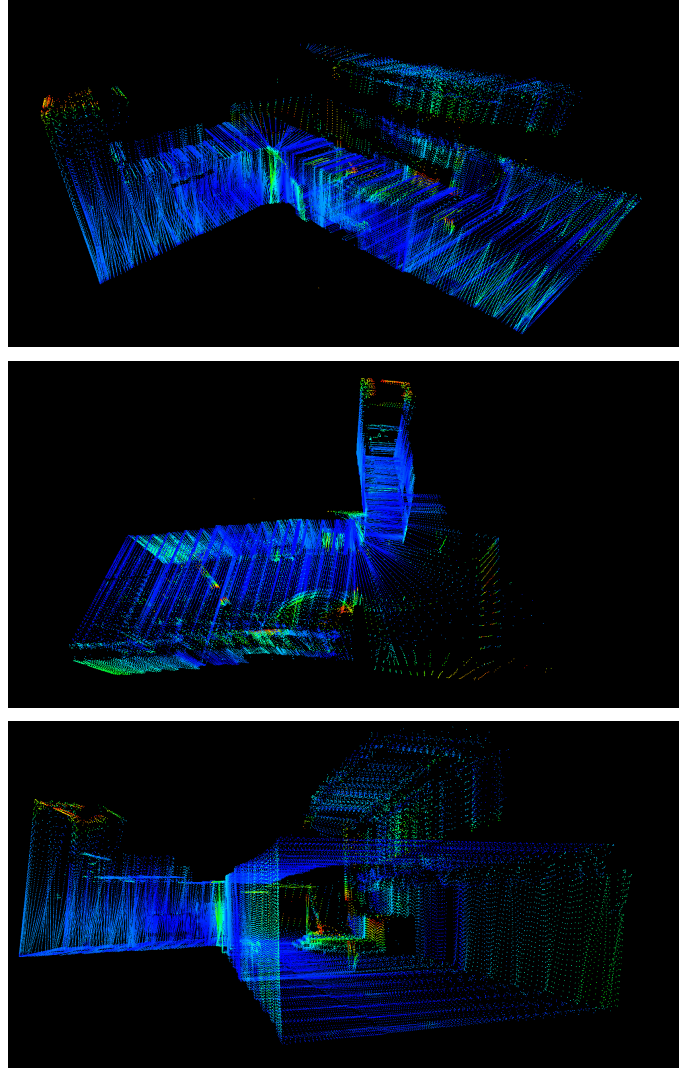


Fig. 6. The three images presented here demonstrate the recorded point cloud. The points are colored according to their deviation from the ground truth point cloud. Note that the corresponding color scale is shown in Fig. 7.

the LiDAR (blue line). Without using the data from the LiDAR, the position estimate becomes completely useless due to a strong drift, which is typical for IMUs in this price range. Consequently, a low-cost LiDAR helps to improve position estimation using IMUs.

7.2 3D-Point-Clouds

The main purpose of this work was not to generate 3D point clouds using LiDAR, however, the position estimation works sufficiently well that this becomes possible. We have created the 3D point cloud as explained previously in section 6.3. No calibration of the LiDAR was performed for the data acquisition. In this experiment, we walked in a relatively straight line along the main corridor of our institute building with a 90 degree curve in the middle while recording the data. We stopped 4 times for a few seconds during data recording. In order to be able to make a comparison, we recorded a point cloud of the same environment using a high-quality, survey-grade Riegl VZ-

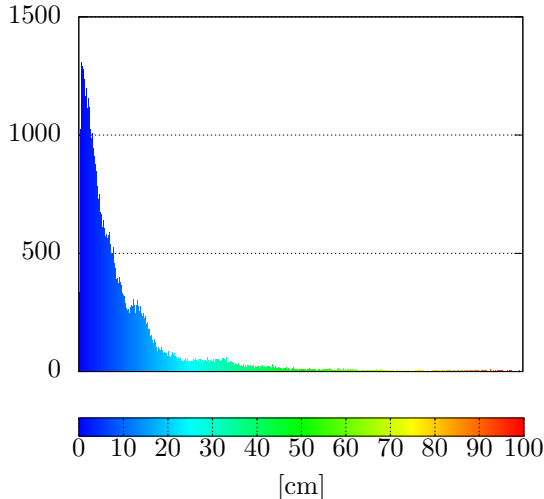


Fig. 7. The x -axis shows the deviation in cm of the point cloud shown in Fig. 6 from the ground truth point cloud. The y -axis shows the number of points. In addition, the color scale is shown, which assigns the deviation to the points from Fig. 6.

400⁵ terrestrial 3D laser scanner as ground truth. The resulting point cloud of our device is shown in Fig. 6. All points are colored according to their point-to-point distance from the true point cloud after rigid registration using the *Iterative Closest Point* (ICP) algorithm. The corresponding color scale and the histogram of the deviations can be seen in Fig. 7. Using the presented method, 90% of all points have a deviation of less than 21.46 cm. 70% of the points have a deviation of less than 9.77 cm. Despite some smaller inaccuracies the general shape of the scene is well represented and there are no obvious deviations from the trajectory leading to a curvature in the 3D point cloud. The points with large deviation (red), seen in the upper left of the first and third image in Fig. 6, are probably due to a window front located there. In the absence of glass in the environment, the deviations are correspondingly smaller.

8. CONCLUSIONS

The purpose of this scientific work was to use data obtained from a LiDAR to improve position estimation by IMUs. The relevance of calibration of IMUs was discussed and a reliable method for calibration was presented. Furthermore, the importance of the exact determination of the orientation was explained and a procedure was presented, which provides reliable results even during movements with high dynamics. A strategy has been developed which makes it possible to detect a standstill and thus to correct the acceleration measurements of the IMU. It has been shown that this method significantly improves the position estimation of the IMU. Moreover, the estimation of the trajectory is sufficiently accurate to determine a 3D point cloud that accurately represents the shape of the environment.

9. FUTURE WORK

Needless to say, a lot of work remains to be done. We are currently working on merging the data from two or more

IMUs, which requires that all IMUs provide the same or at least very similar measurement data. At this time, this is only possible under the condition that both IMUs have exactly the same orientation. In reality however, it will be almost impossible to mount two or more IMUs with the exact same orientation on one platform. Therefore it is necessary to calibrate the exact rotation between the IMUs. If non-linear motions are also to be recorded, the translation must also be known. Furthermore, we are currently developing methods to determine these parameters. At the same time, the LiDAR should be calibrated. Our low-end LiDAR is not well mounted and is eccentric while rotating, so the distance measurements are slightly distorted. This problem is probably due to the low price. Nevertheless, we would like to show how to design a functional 3D scanner using low price technology. We would like to use technologies such as *Simultaneous Localization and Mapping* (SLAM) or loop closing methods to improve the results further. In the future, we will use the method we presented to implement a mapping system for underwater environments. Such a system needs to distinguish between a moving and stationary phases of the remotely operated vehicle (ROV). Also, we aim at developing an autonomous system that creates 3D point clouds inside buildings using a drone, LiDAR and IMU.

ACKNOWLEDGEMENTS

This work was supported through a grant of the Federal Ministry for Economic Affairs and Energy, BMWi (project UWSensor, FKZ: 03SX482A) and the Elite Network of Bavaria.

REFERENCES

- Emter, T. and Petereit, J. (2019). Simultaneous localization and mapping for exploration with stochastic cloning EKF. In *2019 IEEE International Symposium on Safety, Security, and Rescue Robotics (SSRR)*, 164–171.
- Hellmers, H., Diefenbach, N., and Eichhorn, A. (2016). IMU/UWB Sensorfusion für die Indoor-Positionierung von fahrbaren Plattformen. *Zeitschrift für Geodäsie, Geoinformation und Landmanagement (ZfV)*, Wisner, 6, 407–415.
- Madgwick, S. (2010). An efficient orientation filter for inertial and inertial/magnetic sensor arrays. *Report x-io and University of Bristol (UK)*, 25, 113–118.
- McCall, J.R. (2019). *Tracking Using Fusion of Multiple Inertial Measurement Units*. Ph.D. thesis, Honors Theses.
- Tedaldi, D., Pretto, A., and Menegatti, E. (2014). A robust and easy to implement method for IMU calibration without external equipments. In *2014 IEEE International Conference on Robotics and Automation (ICRA)*, 3042–3049. IEEE.
- Valenti, R.G., Dryanovski, I., and Xiao, J. (2015). Keeping a good attitude: A quaternion-based orientation filter for IMUs and MARGs. *Sensors*, 15(8), 19302–19330.
- Wendel, J. (2011). *Integrierte Navigationssysteme: Sensordatenfusion, GPS und Inertiale Navigation*. Oldenbourg Verlag, 2nd edition.
- Wongwirat, O. and Chaiyarat, C. (2010). A position tracking experiment of mobile robot with inertial measurement unit (IMU). In *ICCAS 2010*, 304–308. IEEE.

⁵ <http://riegl.com/nc/products/terrestrial-scanning/>